Revisiting the Holocene global temperature conundrum

Article *in* Nature · February 2023

DOI: 10.1038/s41586-022-05536-w

CITATIONS
88

READS
2,598

2 authors:

Darrell Kaufman
Northern Arizona University
367 PUBLICATIONS **16,147** CITATIONS
SEE PROFILE

Ellie Broadman
United States Geological Survey
13 PUBLICATIONS **138** CITATIONS
SEE PROFILE

Review

Revisiting the Holocene global temperature conundrum

https://doi.org/10.1038/s41586-022-05536-w

Received: 4 May 2021

Accepted: 7 November 2022

Published online: 15 February 2023

Check for updates

Darrell S. Kaufman[1]✉ & Ellie Broadman[1,2]

Recent global temperature reconstructions for the current interglacial period (the Holocene, beginning 11,700 years ago) have generated contrasting trends. This Review examines evidence from indicators and drivers of global change, as inferred from proxy records and simulated by climate models, to evaluate whether anthropogenic global warming was preceded by a long-term warming trend or by global cooling. Multimillennial-scale cooling before industrialization requires extra climate forcing and major climate feedbacks that are not well represented in most climate models at present. Conversely, global warming before industrialization challenges proxy-based reconstructions of past climate. The resolution of this conundrum has implications for contextualizing post-industrial warming and for understanding climate sensitivity to several forcings and their attendant feedbacks, including greenhouse gases. From a large variety of available evidence, we find support for a relatively mild millennial-scale global thermal maximum during the mid-Holocene, but more research is needed to firmly resolve the conundrum and to advance our understanding of slow-moving climate variability.

The average temperature of the surface of the Earth is a key indicator of global warming and a focus of international agreements to limit climate change. A global warming level of 1 °C relative to the late nineteenth century has now been exceeded (Fig. 1a) and warming will probably continue for centuries[1]. A long-term perspective on global mean surface temperature (GMST), including warm periods during the history of the Earth, is needed to contextualize this multicentury global warming[2,3]. To this end, the temperature history of the current interglacial period—the Holocene, beginning 11.7 thousand years ago (ka)—is of particular interest because it provides one measure of the climatic 'safe operating space' for agriculture-based societies[4]. As such, natural variability in GMST during the Holocene may be seen as a baseline against which human influence on climate can be gauged[5].

Evidence for reconstructing and understanding GMST changes is more abundant for the Holocene, and especially the second half of the Holocene, than for any other multimillennial period. Nevertheless, studies of Holocene GMST have reached contrasting conclusions on the millennial-scale temperature trends that occurred before industrialization, confounding the long-term perspective on modern global warming. A landmark reconstruction of GMST showed peak warmth during the mid-Holocene, when GMST reached about 0.8 °C higher than that of the preindustrial period[6]. By contrast, early transient climate modelling showed that GMST was around −0.5 °C colder during the mid-Holocene compared with preindustrial temperature, followed by continued warming[7]. This discrepancy between the late Holocene global cooling trend inferred from proxy evidence versus the warming trend simulated by climate models is known as the 'Holocene temperature conundrum'[7]. The contradiction has challenged both proxy-based palaeoclimate reconstructions and climate model simulations. In response, subsequent studies have attempted to resolve the conundrum by adjusting for possible weaknesses in the proxy data[8], adding plausible forcings to climate models[9,10] or blending data and models[11,12], all arriving at different conclusions about the cause of the conundrum and its solution.

Even before the publication of these recent studies, inconsistent proxy-based and model-based evidence, together with the relatively small magnitude of Holocene climate change, hampered attempts to definitively identify a global Holocene thermal maximum (HTM)[13–16]. Various regional HTMs, which occurred at different times in different places between around 10 and 5 ka, especially at the middle and high latitudes of the Northern Hemisphere, are robust features of temperature reconstructions[17–20] and climate model simulations[21–23]. Although the timing and spatial pattern of regional HTMs afford insights into the dynamical response to climate forcing, this Review focuses on the global HTM as measured by GMST and determined by global-scale climate forcings. Reconstructing GMST—the average temperature of the planet as a whole—is challenging. Empirical evidence from low latitudes and the Southern Hemisphere is generally limited, and only some of the planet was probably warmer whereas other parts were cooler during the global HTM[19,20,24–27]. On the modelling side, none of the 16 latest-generation global climate models that participated in the recent CMIP6-PMIP4, 6-ka experiment[28] simulated GMST that exceeded their preindustrial control runs. GMST at 6 ka in these models averaged 0.3 °C cooler than the preindustrial period (Fig. 1b), arguing against a global HTM. Conversely, other models show that GMST responds sensitively to various forcings (for example, refs. [9,29]), some of which were not fully implemented in PMIP4 climate simulations.

In light of these contrasting results, we review major lines of evidence relevant to reconstructing Holocene GMST. We bring together evidence from proxy data and model simulations to investigate global

[1]School of Earth and Sustainability, Northern Arizona University, Flagstaff, AZ, USA. [2]Present address: Laboratory of Tree-Ring Research, University of Arizona, Tucson, AZ, USA. ✉e-mail: darrell.kaufman@nau.edu

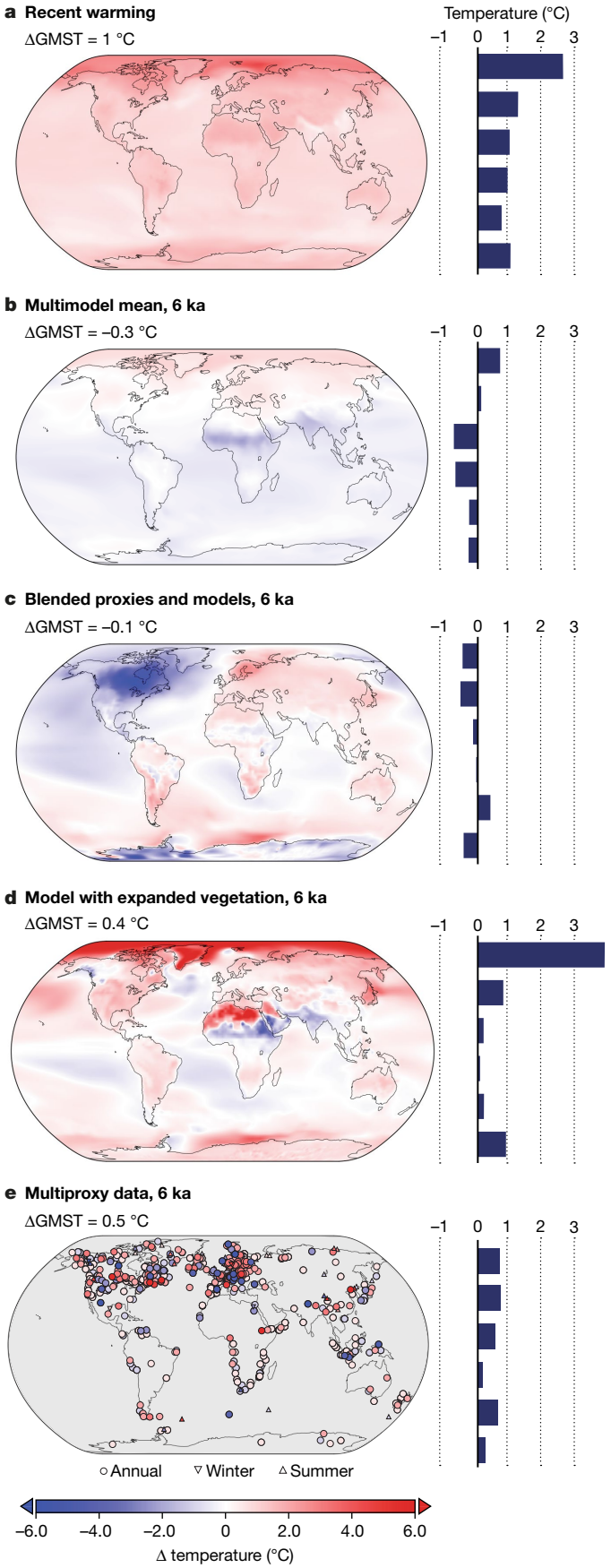

Fig. 1 | GMST anomalies during recent global warming and the mid-Holocene (6 ka) from proxies and models. a, Global warming level of 1 °C relative to 1850–1900 (ref. [1]). **b**, Modelled temperature (CMIP6-PMIP4 multimodel mean) for 6 ka relative to preindustrial[28]. **c**, Blended proxy data and simulated temperature (LGMR data assimilation) at 6 ka relative to 0.5 ka (ref. [11]). **d**, Modelled temperature (CESM1.2) with prescribed expanded vegetation at 6 ka relative to preindustrial[9]. **e**, Proxy records (Temp12k v1.0.2) for 6 ka (6.5–5.5 ka minus 1–0 ka averages), with symbols representing annual, summer and winter temperature (n = 458, 135 and 11, respectively)[34]. Symbols representing sites with less extreme anomalies are in some cases obscured by those with more extreme anomalies, both positive and negative. Plotted using Panoply Data Viewer (NASA Goddard Institute for Space Studies, https://www.giss.nasa.gov/tools/panoply/).

climate indicators, forcings and feedbacks from the perspectives of the atmosphere, ocean and cryosphere, evaluating their overall consistency (Fig. 2). We take a millennial-scale view, consistent with the typical temporal resolution of proxy records. We focus on addressing the heart of the Holocene temperature conundrum: whether GMST decreased or increased during the second half of the Holocene. Specifically, we compare the millennium centred on 6 ka (hereafter, mid-Holocene, MH), a long-standing target for climate model–data comparisons[30], with the millennium that preceded the twentieth century (900–1900, hereafter, last millennium, LM). We implement a consistent reference period, when possible, by comparing both periods (MH and LM) with 1850–1900, which is considered representative of preindustrial conditions[31]. We find that, despite the ever-growing volume and variety of data on Holocene climate, important uncertainties remain. We conclude with a perspective on research priorities to resolve these uncertainties.

Empirical evidence for the global HTM

Temperature reconstructions based on proxy data

A variety of methods have been developed to reconstruct temperatures before the advent of instrumental-based observations. These methods rely on biological and physical changes that are preserved in natural archives on the surface of the Earth, including sediments, glacier ice and speleothems. The changes recorded in these natural archives can be translated to site-level temperature, serving as proxy records of past climate, with important caveats (for example, ref. [32]).

A global compilation of quality-controlled multiproxy records from 470 terrestrial and 209 marine sites (Fig. 1e) was recently used to reconstruct GMST for the Holocene (Temp12k)[33,34] (Fig. 3i). This reconstruction was based on five statistical methods, each with a different approach to averaging the globally distributed proxy records and to characterizing various sources of uncertainty, including proxy-inferred temperature, chronology and methodological choices. For example, two methods first standardized the temperature variance of aggregated proxy data and then restored it to a target, whereas the other three methods used the native variance of the calibrated proxy data. The median of this multimethod ensemble reconstruction shows that the warmest 200-year-long interval before industrialization took place around 6.5 ka, when GMST is estimated to have been 0.7 °C warmer than the nineteenth century. The plausible range of GMST estimates in this ensemble range from 0.3° to 1.8 °C (5th to 95th percentiles). A subsequent slightly expanded proxy data network and an alternative reconstruction method shows an estimated GMST of approximately 0.6 °C around 6.5 ka (ref. [35]). GMST averaged over the millennium centred on 6 ka is lower than those of the warmest centuries (Table 1).

The Temp12k reconstruction is also similar to the first Holocene GMST reconstruction based on both terrestrial and marine proxy data[36]. That study used a smaller dataset (73 sites) and different procedures to estimate a maximum warmth of 0.8 °C ± 0.3 °C (2σ) relative to 1850–1900 at around 7 ka. Furthermore, these GMST reconstructions are consistent with two others based on extensive compilations of sea-surface temperature (SST) records alone[11,37], both of which show a

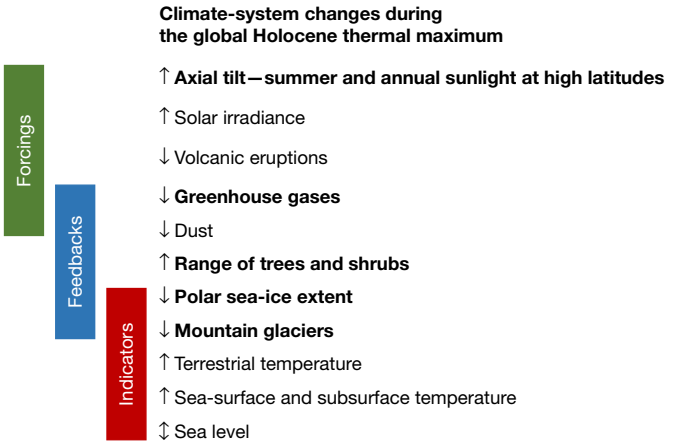

Fig. 2 | List of climate-system features and metrics discussed in this Review. Elements are arranged with global climate forcings at the top and global climate indicators at the bottom. In between are climate feedbacks arranged by the extent to which they are estimated to influence versus indicate global climate during the HTM. Arrows show the direction of change during the HTM relative to the last millennium. Bold text indicates high confidence in the change; plain text indicates lower confidence.

prominent global HTM and roughly 0.5–1 °C of cooling across the middle and late Holocene, although ref. [11] emphasizes that their proxy-only reconstruction is hampered by sparse data coverage in some latitudinal bands. The SST proxy data agree with a reconstruction of ground temperature from globally distributed boreholes, which indicates peak warming of about 1–2 °C at 6–7 ka relative to 1960–1991 (ref. [38]). The relation between ground temperature and surface air temperature is complicated, however, by the varying extent of insulating seasonal snow cover[39]. Another recent reconstruction focused on a globally distributed pollen-only dataset shows maximum temperatures extending from around 8 to 5 ka when GMST was roughly 0.5 °C above the late Holocene minimum (1 ka)[20]. The use of pollen for reconstructing temperature during the late Holocene has been challenged because of human effects that might decouple vegetation composition from the associated climate interpretation[40]. Late Holocene cooling is not only evidenced by pollen data, however; it is a prominent feature of other terrestrial and marine proxy types[34,41] (Fig. 3k,m). At the continental scale, pollen records show that annual temperature over North America and Europe cooled by at least 0.5 °C after 5.5 ka (ref. [42]), consistent with the early recognition of the 'hypsithermal interval', which was based on pollen assemblages in Europe[43]. In contrast to these proxy-data compilations that support the occurrence of a global HTM, earlier reconstructions based on selected proxy types indicate that MH land and ocean surface temperatures were indistinguishable from preindustrial climate[15]. Considering several lines of proxy-based evidence, the Sixth Assessment Report of the Intergovernmental Panel on Climate Change (IPCC) estimated, with medium confidence, that GMST averaged over the warmest centuries of the global HTM was 0.2–1 °C higher than 1850–1900 (ref. [44]).

Mountain glaciers

The size of mountain glaciers is sensitive to the temperature and duration of the melt season. For maritime and low-latitude glaciers, the melt season can extend over most of the year[45]; at higher latitude, a warmer and longer melt season factors into mean annual temperature such that glacier size globally can be used to track GMST[46]. Moraines and other dated glacial-geomorphic features can be used to estimate the timing of glacier retreat and surface deposits derived from nonglacial sources can be used to determine the ages of ice-free periods.

To summarize the global pattern of Holocene mountain glacier history for this Review, we used a compilation of glacial-geomorphic and geochronological data from 189 globally distributed glaciers[47]. We derived a glacier extent index by assigning values to the qualitative status of each glacier and then averaged these values in 100-year intervals for four large-scale regions. This rudimentary summary of relative glacier extent indicates that glaciers generally retracted to their Holocene minima between 10 and 6 ka (Fig. 3l). Glacier advances were underway in mountains of both hemispheres between 5 and 3 ka (ref. [48]), during the period referred to as the Neoglacial[49]. The general pattern of less ice during the MH and expanded ice during the LM also applies to the Greenland ice sheet[50] and possibly to the West Antarctic Ice Sheet, which seems to have readvanced during the second half of the Holocene[51].

Ocean subsurface temperature

Approximately 91% of the heat energy generated by recent global warming has been stored in the ocean[1]. This heat exchange between the ocean and atmosphere means that ocean heat content and GMST are strongly related (for example, ref. [52]). This correspondence was probably strong at the millennial scale during the second half of the Holocene when changes were relatively minor in ocean and ice-sheet volumes, land surface area and ocean circulation. Marine proxy records of subsurface temperature generally show that the MH was warmer than the LM (Fig. 3). For example, several proxy records from diagnostic locations in the equatorial Pacific and subtropical Atlantic Ocean indicate that intermediate waters were 2 ± 0.5 °C warmer during the early Holocene than during the preindustrial late Holocene, which exceeds the cooling at the overlying surface[53] (Fig. 3m). Although temporal resolution is lower, a compilation of marine proxy records indicates that deep ocean temperatures decreased by an average of about 0.5 °C following an early Holocene maximum[37] (Fig. 3m). Noble gas thermometry from two Antarctic ice cores has been used to reconstruct the total heat content of the global ocean[52,54], indicating that heat energy reached a maximum during the early Holocene, followed by little change or possibly slight cooling thereafter (Fig. 3n).

Common Era temperature

Many regional studies based on documentary and proxy evidence show that the coldest decades and centuries of the past 1 to 2 kyr generally occurred between the fifteenth and nineteenth centuries, during the period known as the Little Ice Age (LIA) (for example, ref. [55]). Although the extent and timing of LIA cooling varied regionally, its global-scale imprint is evident in compilations of multiproxy records that together show a robust millennial-scale cooling trend of approximately 0.1–0.2 °C per 1,000 years over the past 2 kyr from extensive, quality-controlled marine[56], terrestrial[57] and global[58] datasets. This proxy-inferred cooling is supported by the global expansion of glaciers[59] and by temperature profiles measured in globally distributed boreholes[60]. From this perspective, the LIA is the extension of the multimillennial cooling trend that followed the global HTM.

Summary of empirical evidence

The global HTM is apparent in several compilations of globally distributed terrestrial and marine proxy datasets, including compelling evidence for global cooling over the Common Era before industrialization. Mountain glaciers worldwide generally retreated during the early and middle Holocene and readvanced thereafter. Similarly, subsurface ocean waters were probably warmer during the first half of the Holocene than during the second.

Holocene climate forcings and feedbacks

The following sections are presented roughly in order of assumed importance for influencing Holocene GMST.

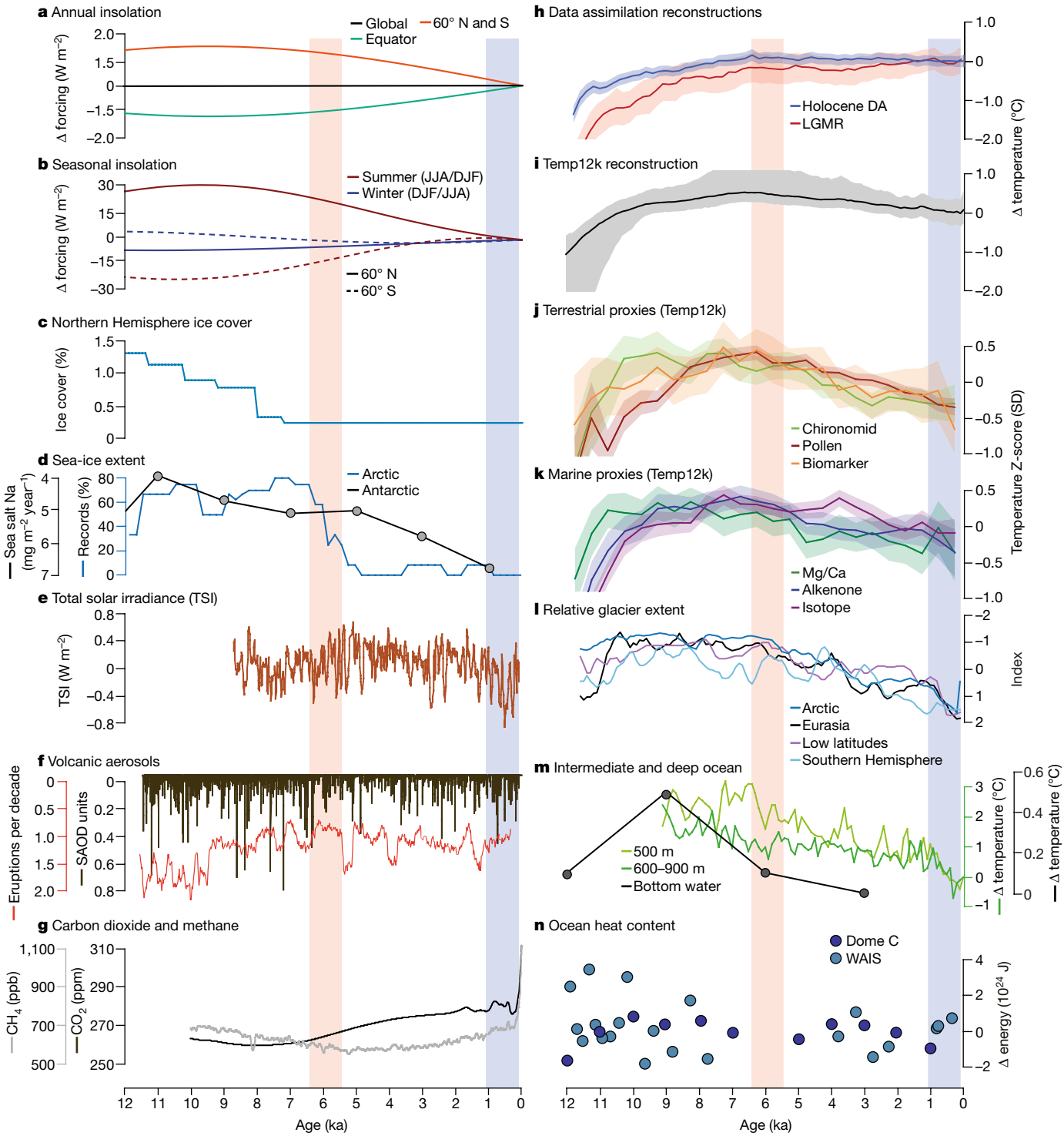

Fig. 3 | Holocene climate forcings and feedbacks (left) and selected reconstructions and proxy data (right). **a**, Annual insolation at 60° N, 0°, 60° S and globally[61]. **b**, Seasonal (JJA and DJF) insolation at 60° N and 60° S (ref. [61]). **c**, Northern Hemisphere ice cover[142]. **d**, Sea-ice extent for the Arctic (percentage of records indicating low sea-ice concentration in ref. [85]) and the Antarctic (flux of sea salt sodium at Dome C[88]). **e**, Total solar irradiance inferred from cosmogenic isotope abundance[106]. **f**, Volcanic SAOD and number of eruptions per decade (three-decade running mean) inferred from sulfate aerosols in polar ice[114]. **g**, Concentrations of atmospheric CO_2 and CH_4 in Antarctic ice cores[99]. **h**, LGMR[11] and Holocene data assimilation (DA)[12]; solid line and shading are the mean and ±1σ uncertainty. **i**, Temp12k GMST reconstruction[33]; solid line and shading are the median and 90% range of ensemble members. **j**, Composites for terrestrial proxy types from the Temp12k database[34]: pollen, chironomids and biomarkers (excluding alkenones); solid line and shading are the mean and 95% confidence interval. The spatial–temporal structure of each proxy type is examined in ref. [20]. **k**, As in **j** but for marine proxy types: Mg/Ca, alkenones and isotopes (isotope records are almost exclusively marine). **l**, Mountain glacier extent summarized from individual glacier histories in ref. [47] averaged by four latitudinal zones: Arctic (n = 73), Eurasia (n = 54), low latitudes (n = 24) and Southern Hemisphere (n = 38). Relative size classified as: 3 = Holocene maximum, 2 = advancing, 1 = glacier present, −1 = retreating, −2 = smaller than twentieth century, averaged and 300-year smoothed. **m**, Reconstructed temperature of global bottom water[37] and Indonesian Throughflow water, which is linked to North Pacific and Antarctic intermediate waters[143]. **n**, Reconstructed total ocean heat content based on noble gases from Dome C[54] and the West Antarctic Ice Sheet (WAIS)[52]. Red vertical bar indicates mid-Holocene (6.5–5.5 ka); blue bar indicates last millennium (900–1900). Δ values are changes relative to the 1850–1900 preindustrial reference period.

Table 1 | Primary global climate forcings and indicators for the mid-Holocene and the last millennium

	Mid-Holocene (6.5–5.5 ka)	Last millennium (900–1900)	Reference period	Selected refs.
Climate forcing and feedbacks				
Insolation, annual global ($W m^{-2}$)	0	0	1850–1900	Laskar[61]
Insolation, annual 60° N and 60° S ($W m^{-2}$)	1.2	0.1	1850–1900	Laskar[61]
Insolation, annual 0° N/S ($W m^{-2}$)	−1.0	−0.1	1850–1900	Laskar[61]
Insolation, JJA 60° N ($W m^{-2}$)	21.9	1.0	1850–1900	Laskar[61]
Atmospheric CO_2 (ppm)	−25.3±1.3	−9.1±3.0	1850–1900	Köhler[99]
Atmospheric CH_4 (ppm)	−0.23±0.01	−0.13±0.04	1850–1900	Köhler[99]
Radiative forcing, well-mixed GHG ($W m^{-2}$)	−0.76±0.03	−0.30±0.09	1850–1900	Köhler[99]
Radiative forcing, total solar irradiance×0.13 ($W m^{-2}$)[a]	0.01±0.03	−0.03±0.04	1850–1890	Wu[106]
Radiative forcing, volcanic SAOD×20 ($W m^{-2}$)[b]	−0.04±0.40[c]	−0.06±0.38[c]	1850–1900	Sigl[114]
Radiative forcing, volcanic frequency (no. per decade)	0.96	1.11	1850–1900	Sigl[114]
Land-cover (vegetation) albedo	Decreased	Baseline	LM	Prentice[73]
Arctic sea-ice cover and albedo	Decreased	Baseline	LM	Stranne[85]
Antarctic sea-ice cover and albedo	Decreased	Baseline	LM	Wolff[88]
Dust abundance (deposition)	Decreased	Baseline	LM	Albani[79]
GMST (°C)				
Proxy-based, multistudy, IPCC-assessed range	0.2–1.0[d]	0.03±0.09[c]	1850–1900	Gulev[44], PAGES 2k[105]
Multiproxy, multimethod Temp12k	0.47[e], 0.6 (0.3, 1.5)[f]	Not reviewed	1850–1900	Kaufman[33]
Pollen only, LegacyClimate+Temp12k	0.48[g]	Not reviewed	1 ka	Herzschuh[19]
SST proxy system models, scaled to GMST	0.75±0.17[e]	Not reviewed	1850–1900	Osman[11]
SST proxies adjusted for local seasonal insolation	−0.24[e]	Not reviewed	1850–1900	Bova[8]
Data assimilation, SST proxies and time-slice model prior	−0.14[e], −0.25[h]	Not reviewed	1850–1900	Osman[11]
Data assimilation, Temp12k proxies and transient model prior	0.12[e], 0.20[e,i]	Not reviewed	1850–1900	Erb[12]
Simulated, CMIP6-PMIP4 multimodel mean[j]	−0.3±0.1[k]	Not reviewed	Preindustrial control	Brierley[28]
Simulated, CESM1.2 with expanded vegetation[j]	0.42±1.6	Not reviewed	Preindustrial control	Thompson[9]
Seasonal cycle as an analogue for climate variability	≤0.1	Not reviewed	Preindustrial control	Laepple[72]
Ocean subsurface temperature				
Intermediate water	Higher	Baseline	LM	Rosenthal[53]
Bottom water	Higher	Baseline	LM	Shakun[37]
Global ocean heat content	Equivocal	Baseline	LM	Baggenstos[52]
Ice volume and sea level				
Global mountain glacier extent	Smaller	Larger	Twentieth century	Solomina[47,59]
Greenland ice sheet	Smaller	Larger	Twentieth century	Briner[50]
Antarctic ice sheet	Equivocal	Equivocal	Twentieth century	Jones[128]
GMSL	Equivocal	Not reviewed	Twentieth century	Gulev[44]

[a]Total solar irradiance converted to effective radiative forcing using assessed scaling and adjustments of ref. [107].
[b]SAOD converted to $W m^{-2}$ using the scaling of ref. [107].
[c]Calculated using decadal averages.
[d]Warmest centuries between 7 and 6 ka (very probable range), medium confidence.
[e]Difference between millennia centred on 6 and 0.5 ka; added 0.03 °C to adjust GMST of the last millennium to the 1850–1900 reference period, based on the reconstruction of the PAGES 2k Consortium[105].
[f]Warmest millennium in the ensemble median centred on 6.5 ka (5th and 95th percentiles) relative to 1800–1900 (subtract 0.03 °C to adjust to the 1850–1900 reference period).
[g]Difference between 500-year smoothed maximum GMST at 5.2 ka and 1.0 ka.
[h]Ensemble trend between 7 and 0.1 ka.
[i]Data assimilation with assumed proxy uncertainties reduced by 20%.
[j]Global surface air temperature; the IPCC assessed global surface air temperature and GMST as differing by less than 10% (ref. [44]).
[k]Mean±1σ of 16 models.

Orbital forcing

During the Holocene, the overall change in average annual global insolation was minimal (−0.01 W m^{-2} since the MH)[61] (Fig. 3a), as the deceasing trend at high latitudes was balanced by the increasing trend at low latitudes. However, strong seasonal trends (Fig. 3b) drove feedbacks that influenced GMST (for example, ref. [62]). According to the Milankovitch theory, global glacial periods are triggered as summer insolation declines at northern high latitudes, increasing planetary albedo through the ice–albedo feedback. Summer insolation at 60° N, the latitude that represents a large proportion of the Northern Hemisphere land area, reached its Holocene maximum in summer (JJA) and began to decrease at around 10 ka (ref. [61]). However, slow-responding components of the climate system continued to warm the surface of the Earth. Remnants of Pleistocene ice sheets lingered until 9 ka in Scandinavia[63] and until around 6.7 ka in North America[64] (Fig. 1c). By

the end of the first half of the Holocene, declining summer insolation at 60° N was the overriding control on GMST. By the MH, summer (JJA) insolation at this latitude had decreased by 8.4 W m^{-2} relative to its Holocene peak but was still 21.9 W m^{-2} higher than 1850–1900 (ref. [61]).

The influence of insolation forcing on temperature is evidenced by trends in proxy-based reconstructions that correlate with local insolation changes, both annually and seasonally. During the MH, annual insolation at high latitudes in both hemispheres was higher than during the LM, whereas the trend in the tropics was generally opposite (Fig. 3a). This caused the latitudinal insolation gradient in the Northern Hemisphere to steepen as reflected in the Temp12k dataset by nearly flat temperature trends across the 30° N to 30° S latitude during the past 10 kyr (ref. [33]), as well as by the steepening proxy-reconstructed temperature gradient between the MH and the LM[65]. The role of local insolation forcing is further evidenced by winter-dominated temperature proxy records that correlate with local, winter insolation changes. A cold-season warming trend from the MH to the LM has been inferred from multiproxy geochemical indicators at northern high latitudes[66–69], consistent with increasing winter (DJF) insolation at 60° N. Higher winter temperature at northern high latitudes during the LM relative to the MH would have diminished the magnitude of the HTM, but not overwhelmed it, consistent with the Milankovitch theory. A contrasting view from a recent pollen-based reconstruction shows that winter temperatures cooled across the Northern Hemisphere following the MH[70].

Single-forcing climate model experiments have been used to better understand the cause of late Holocene warming simulated by most climate models. Orbital-forcing-only runs by ref. [9] using three transient simulations over the past 20 kyr showed little GMST change. In one model, however, GMST rose to about 0.2 °C above preindustrial at around 6 ka. This model result agrees with another sensitivity experiment of orbital forcing alone showing that, as obliquity decreases, as it did after around 9 ka, GMST decreases in response to cloud and seasonal sea-ice feedbacks[71].

Finally, an innovative conceptual model of insolation-driven temperature uses the modern seasonal cycle to relate insolation to local temperature response, thereby including nonlinearities analogous to those that operate on orbital timescales[72]. The model, which accounts for fast feedbacks only, shows that GMST declined slightly (≤0.1 °C) over the past 6 kyr. Including long-term processes would result in a stronger climate response.

Vegetation and dust

Changes in terrestrial vegetation and atmospheric dust during the Holocene have been reconstructed from proxy records and their effects on climate have been investigated using models. Pollen-based vegetation reconstructions show that Saharan Africa was green during the MH and that forest cover was more extensive regionally at middle and high latitudes of the Northern Hemisphere than during the LM[73,74]. A recent transient simulation by an Earth system model captures the main trends in biome shifts during the MH and places them in the context of climate dynamics[75]. These range shifts warmed the Northern Hemisphere land surface by decreasing its albedo during summer, through sea-ice feedbacks during autumn and winter, and through snow-albedo feedbacks in spring[76], collectively resulting in regional temperature changes similar in magnitude to those caused by orbital forcing[77]. Early simulations of 6-ka climate using a model of intermediate complexity showed that GMST increased by 0.9 °C when vegetation changes were included[29]. Recent simulations using a CMIP6-class model[9] show that GMST was roughly 0.4 °C higher than the preindustrial when vegetation expansion is included (Fig. 1d). The prescribed vegetation expansion in this model probably represents the high end of the Holocene vegetation change and, therefore, the resulting temperature response. When sampled at the same locations as the Temp12k proxy data network, the MH is even warmer in the model than estimated by the proxy data. Furthermore, following the global HTM, anthropogenic land-cover change increased surface albedo, causing an estimated 0.17 °C of global cooling[78].

The expansion of vegetation during the MH also reduced the source area for mineral dust, consistent with proxy evidence for less atmospheric dust loading during the MH than the LM[79]. This reduced dustiness might have contributed to the global HTM mainly by decreasing the scattering of solar radiation[80], although the simulated effect of dust on GMST differs among climate models. One simulation shows that removing all atmospheric dust causes a 0.3 °C decrease in GMST at 6 ka compared with the preindustrial control[10]; however, the model did not include important long-wave feedbacks. Those that do, generally show limited effects[9,81–83].

Sea ice

Retreating sea-ice extent decreases planetary albedo and allows heat transfer from the ocean to the atmosphere, amplifying global warming[84]. Most proxy records indicate that sea-ice cover was less extensive during the MH compared with the LM across much of the Arctic Ocean[85], but not all[86,87]. Sea-ice cover was also reduced in the Southern Ocean during the MH and increased after[88,89] (Fig. 3d), although evidence is limited. Climate model simulations for 6 ka (refs. [90,91]) and a transient Holocene simulation[92] show that increased insolation at northern high latitudes causes a reduction in Arctic sea-ice cover and that the resulting warming extends into winter across the hemisphere. Several simulations of changing sea-ice extent also show a remote-warming response that extends to the extratropics and tropics through dynamical circulation changes (for example, refs. [93,94]). Simulations also indicate that, when sea ice is less extensive than current conditions, GMST increases in response (for example, refs. [95–97]), such as might have occurred during the global HTM.

Greenhouse gases

The atmospheric concentration of well-mixed greenhouse gases (GHGs) is a primary control on GMST through the Cenozoic[98] but GHG changes during the preindustrial Holocene were relatively minor. Air trapped in polar glacier ice contains about 16 ppm less CO_2 during the MH than during the LM[99] (Fig. 3g and Table 1). By comparison, this is less than atmospheric CO_2 build-up during the eight years between 2011 and 2019 (about 19 ppm)[44]. The concentration of CH_4 was also lower during the MH than the LM. Together, the lower concentrations of CO_2, CH_4 and N_2O caused an estimated reduction in radiative forcing of about 0.46 W m^{-2} during the MH compared with the LM[99]. To put this into perspective, by decreasing the CO_2 concentration by 20 ppm in the PMIP4 MH (6 ka) experimental protocol, the ensemble mean GMST averaged −0.2 °C colder than in PMIP3 models, which used preindustrial GHG levels[28].

Several hypotheses have been put forward to explain the increase in GHG concentrations from the MH to the LM (for example, ref. [100]). One prominent hypothesis attributes the increase to land-use practices of preindustrial societies[101]. The increase, albeit minor, was sufficient to counterbalance some of the global cooling driven by orbital cycles and to prolong the current interglacial period[102]. Although this increase in GHG concentrations may have staved off the ensuing ice age, humans did not reverse the trend of the orbitally driven cooling until industrialization, beginning in the mid-nineteenth century[103].

Solar and volcanic forcings

Changes in the output of the Sun and the frequency of large volcanic eruptions have substantially affected GMST at annual and decadal scales over the Common Era (for example, refs. [104,105]); their cumulative effects over longer periods are uncertain. A reconstruction of total solar irradiance (TSI) extending back to 9 ka (ref. [106]), which incorporates revised cosmogenic isotope datasets and improved models for production and deposition of cosmogenic nuclides, shows that TSI during the MH was similar to the LM, with a marginally higher mean

(Table 1 and Fig. 3e). A linear regression from 6 ka to 1850 returns a significant ($P < 0.01$) trend of -0.06 ± 0.01 W m^{-2} per 1,000 years, implying a minimal contribution from solar forcing to post-HTM cooling. Effective radiative forcing is estimated to be about 13% of the change in TSI[107], meaning that the difference in the mean values between the two periods equates to roughly -0.04 W m^{-2}. By contrast, many proxy-based studies have attributed century-scale to millennial-scale Holocene climate fluctuations[108–110], as well as climate events[111,112], to solar variability, suggesting an outsized influence beyond that of the estimated effective radiative forcing. Finally, the millennium with the highest nitrate concentration in Antarctica ice, an alternative indicator of solar activity, was high from 6.5 to 5.5 ka (ref. [113]).

A new compilation of global volcanic sulfur emissions, based on aerosol content in ice cores from Greenland and Antarctica, provides the most complete available documentation of Holocene volcanic eruptions that affected global climate (HolVol)[114]. Reconstructed stratospheric aerosol optical depth (SAOD) (Fig. 3f) indicates that global volcanic forcing during the MH was on par with that of the LM. The difference in the mean values between the two periods equates to a radiative forcing of about -0.02 W m^{-2}, based on the conversion from ref. [107]. Although the magnitude of the millennial-scale trend is small, a linear regression from 6 ka to 1850 shows a significant ($P < 0.02$) increase in volcanic forcing. Furthermore, model simulations have shown that the clustering and pacing of volcanic eruptions affects the duration of their cooling effect; it can lead to century-scale cooling by reducing ocean heat content and activating ice–albedo feedbacks[115–117]. Indeed, the number of volcanic eruptions in the HolVol dataset increases from 6 ka to 1850 ($P < 0.01$) based on the annual running average of multidecadal eruption frequency. This result is robust across various multidecadal-scale intervals. A recent Holocene-long transient simulation that includes solar and volcanic forcing attributed the global cooling across the preindustrial Common Era largely to the effects of volcanic aerosol forcing, which were amplified by sea-ice feedbacks[92].

Summary of forcings and feedbacks

There is strong model-based and proxy-based evidence that orbital forcing was the dominant influence on millennial-scale trends in Holocene GMST before industrialization. This forcing drove important feedbacks through decreased polar sea ice and shifted vegetation ranges, which increased GMST above preindustrial levels during the MH. Following the MH, increasing albedo from land-cover changes, together with weakly decreasing solar irradiance and increasing volcanic activity, each perhaps leveraged by slow feedbacks, led to global cooling, which more than counterbalanced the effect of increasing GHGs.

Challenges to the global HTM

Summer bias in proxies

Middle and late Holocene cooling inferred from proxy records generally coincides with decreasing boreal summer insolation. Some authors have used this correlation, along with evidence that some proxies are influenced by seasonal ecological controls (for example, ref. [118]), to conclude that proxy records dominantly reflect summer conditions[8,42,7]. Others emphasize that summer conditions persist into the fall and winter in response to feedbacks and slow-moving features of the climate system[92,119]. As such, mean annual temperature can be both dominated by strong changes in summer and faithfully recorded by proxies. This perspective is supported by sensitivity testing using two different data assimilation procedures, both of which found relatively minimal influence of proxy seasonal bias on temperature reconstructions[11,12]; it is also consistent with proxy-based reconstructed global winter temperature, which decreased during the middle and late Holocene[35].

The assumption that proxy records are dominated by summer insolation is not supported by evidence from the Southern Hemisphere and global oceans. If proxies are summer-biased and driven by local insolation, then they should exhibit opposite Holocene trends in the two hemispheres, tracking changes in summer insolation (Fig. 3b). Proxy records from the high latitudes of the Southern Hemisphere, however, generally do not show overall warming across the Holocene[33]. The timing of peak Holocene warmth varied around the globe but occurred at roughly the same time in both hemispheres[11,120], providing further evidence that proxies calibrated to represent annual temperature are not overwhelmingly biased by seasonal temperature.

The ability of proxy records to faithfully represent annual temperature is further supported by their similar trends across several proxy types from marine and terrestrial sources, most of which peak between 8 and 6 ka (refs. [20,34]) (Fig. 3j,k). The replicability across proxy types, including global glacier extents (Fig. 3l) and subsurface ocean temperature (Fig. 3m), adds confidence to the robustness of the shared trend because they are governed by different underlying biological and physical processes and are sensitive to different seasonal conditions. Moreover, the proxy-only reconstruction of ref. [11], which circumvents many of the issues related to seasonality by using proxy system models, shows a strong global HTM.

Reference [8] recently argued that the global HTM reconstructed by previous studies using proxy data is an artefact of seasonal bias. They assumed that millennial trends in proxy records of Holocene SST are seasonally biased if the records correlate better with local seasonal insolation than with the local mean annual insolation. They then used these inferred seasonalities and the statistical relations between seasonal and annual insolation to adjust the Holocene proxy records to follow their assumptions. This approach demonstrated that a seasonal bias could account for the reconstructed warming during the first half of the Holocene and cooling thereafter, but it did not prove that this trend was caused by seasonally biased proxies. Furthermore, they characterized their 40° S to 40° N SST-only reconstruction as representing global trends, because SST trends in this region correlate with global SST changes in a transient climate model simulation. Because low latitudes warmed less than higher latitudes during the MH, however, the latter must be included when estimating GMST. One commentary (ref. [121]) argued that focusing on local insolation overlooks important climate feedbacks, especially sea-ice albedo, that shape temperature evolution during interglacials. Another commentary (ref. [122]) showed that the outcome of the method (removing thermal maxima) is essentially predetermined by the underlying assumptions, some of which seem unsubstantiated. Among their rebuttals[123,124], the authors stressed the importance of proper site selection when applying their method.

Data assimilation

Data assimilation integrates information from both proxy records and climate model simulations to generate a reconstruction that is consistent with both types of evidence and is constrained by realistic dynamical features of the climate system. However, for the MH, when climate model output diverges from proxy data, data assimilation has not shown which line of evidence is more correct. A recent data assimilation reconstruction[11] extending from the Last Glacial Maximum to the present is based on an extensive compilation of geochemical proxy records of SST (driven by proxy system models), along with time-slice output from an isotope-enabled climate model (Figs. 1c and 3h). The data assimilation ensemble reconstruction shows that the MH was colder than preindustrial, with a small (0.25 °C) but notable warming from 7 ka until the twentieth century[11] and even less warming when considering the millennium centred on 6 ka (Table 1). However, the lack of terrestrial proxy data, or other methodological choices (for example, design of the model prior), could have reduced the MH warming in this data assimilation reconstruction. This assertion is supported by more recent data assimilation GMST reconstructions of the Last Glacial Maximum[125] and Holocene[12] (Fig. 3h), both of which are warmer than that of ref. [11]. The new Holocene data assimilation reconstruction[12] blends the Temp12k database with output from transient climate model simulations. Rather

than a warming trend, this data assimilation reconstruction shows a minor global HTM, with a maximum millennial-scale GMST of about 0.1 °C relative to the late nineteenth century. Sensitivity tests show that the estimated GMST for the HTM increases as the assumed uncertainty in proxy values is reduced; for example, a 20% reduction in uncertainties increases the GMST anomaly to 0.2 °C. MH warmth is present in 88% of the ensemble members of this data assimilation reconstruction. The GMST reconstructions based on data assimilation by both ref. [11] and ref. [12] are notably flat over the middle and late Holocene (Fig. 3h). This might reflect the tendency of data assimilation to underestimate temporal variability, particularly when and where the data network is sparse[126]. For example, of the six reconstruction methods used by the PAGES 2k Consortium to estimate GMST over the Common Era[105], the data assimilation reconstruction is by far the smoothest.

Sea level

The global mean sea level (GMSL) reflects the combined effects of ocean temperature and global ice volume. Reconstructions that depict rising GMSL through the Holocene have been used as evidence against the global HTM (for example, refs. [8,41]). They are based on the commonly accepted model that the Antarctic ice sheet, the biggest potential contributor to GMSL during the second half of the Holocene, is smaller now than at any time during the Holocene. This view is now challenged by theory and by scattered evidence for late Holocene readvances in Antarctica[127,128]. Other challenges arise when translating the elevation of palaeo sea-surface indicators into GMSL because glacial isostatic adjustment and local vertical motion were the dominant controls on local sea level during the Holocene[129]. Models tuned to both near-field and far-field relative sea-level data yield GMSL estimates between about −4 and −1 m for the MH (for example, ref. [130]). By contrast, some studies of far-field locations, where the effects of glacial isostatic adjustment are small and local sea level is expected to approximate GMSL to within about 1 m (for example, ref. [131]), suggest that GMSL was higher during the MH than during the LM (for example, refs. [132,133]). Finally, marine geochemical proxies of total global ice volume have insufficient resolution to constrain the height of GMSL during the MH. In sum, the possibility that GMSL was higher during the MH than the LM cannot be excluded.

Summary of challenges

Of the two recent GMST reconstructions that lack a global HTM, one (ref. [8]) was driven by presupposed local seasonal effects and excluded data from poleward of 40° latitude, where warming was most pronounced, and the other—a data assimilation reconstruction (ref. [11])—contrasts with a more recent data assimilation reconstruction (ref. [12]) that features a minor global HTM, demonstrating the sensitivity of the data assimilation method to assumptions and choice of underlying climate model runs. Evidence for lower GMSL during the MH is too tenuous to argue against the global HTM.

Conclusion

Proxy data that represent a large variety of natural processes operating in disparate settings, sensitive to different seasonal conditions and distributed globally, point in a similar direction. The most parsimonious interpretation is that they track GMST. GMST probably peaked some time late during the first half of the Holocene, at roughly 6.5 ka, as evidenced by extensive proxy data and supported by theory and models. Proxy evidence reported in several studies indicates that GMST was roughly 0.5 °C higher during this millennial-scale period compared with 1850–1900, with most of the warming occurring at middle to high latitudes in the Northern Hemisphere. GMST estimates are typically higher for century-scale changes than for millennial averages, whereas those based on data assimilation methods show nearly no change. The occurrence of a global HTM during the MH is further evidenced by subsequent cooling in both hemispheres during the late Holocene, including proxy records of cryosphere extent and subsurface ocean temperature. The cooling culminated in the LIA, which is well documented globally, on land and in the oceans. This post-HTM cooling coincided with small millennial-scale decreases in solar irradiance and overall increases in both stratospheric aerosols from major volcanic eruptions and the decadal frequency of these eruptions. Late Holocene cooling is also consistent with the Milankovitch theory, which ascribes the onset of global glaciations to climate feedbacks driven by declining summer insolation at northern high latitudes. Sensitivity studies using climate models show that GMST higher than that of the late nineteenth century can be attributed to Arctic amplification of orbital forcing through sea-ice feedbacks, combined with lower land-surface albedo caused by the expansion of dark vegetation. The atmospheric concentrations of well-mixed GHGs increased slightly across the late Holocene but their effect on GMST was apparently overshadowed by other forcings and their attendant feedbacks. Although our preferred interpretation is that GMST decreased during the six millennia before industrialization, more research is needed from both the proxy data and climate modelling perspectives to firmly resolve the conundrum.

Future directions

Resolving possible shortcomings in proxies

If our preferred interpretation is incorrect and GMST never rose above preindustrial levels following the last ice age, then we need to improve our understanding of the temperature signal in proxy records and to further develop our data analytical tools to extract global trends with greater fidelity. Proxy indicators of global-scale conditions, including ocean heat content and GMSL, are fundamental to understanding the evolving net energy balance of the Earth and deserve special consideration. Specifically, higher-resolution measurements of noble gases in Antarctic bubble ice could improve the reconstruction of Holocene ocean heat content. Further near-field constraints are needed to reconstruct Antarctic ice sheet fluctuations, the probable control on global sea level during the second half of the Holocene. This will bolster studies of ice-sheet sensitivity to warming and feed new approaches to jointly model ice-sheet volume, glacial-isostatic adjustments and the viscosity structure of the Earth (for example, ref. [134]).

Apart from global-scale indicators, we must rely on a geographically distributed network of sites to estimate the global mean. Here, filling data gaps is critical to reconciling spatial and seasonal biases, especially given that seasonal biases can be highly regional. More records using a variety of proxy types are especially needed from the Southern Hemisphere, because the current sparse data coverage there leads to marked uncertainties related to spatial averaging. This issue may be more important than seasonal bias, a frequently cited weakness, in solving the Holocene temperature conundrum[11].

Nonetheless, more work is needed to understand how the evolving annual cycle of the Holocene is represented spatially and in different proxy types, with more careful attention directed to defining seasonality itself[135]. Proxies that target different seasons can be used together to develop better estimates of annual conditions. Proxy system models are also on the rise[136] and their further development is needed to circumvent issues related to inverse models used for proxy calibration, including seasonality effects, and to bridge the gap between native proxy data and climate model output, including in data assimilation[137]. New advances in analytical capabilities might help resolve seasonal variations in proxy records, thus circumventing the seasonality challenge (for example, ref. [138]).

Whether large-scale reconstructions are based on conventional or emerging approaches, there is an urgent need to improve the reusability of palaeoclimate proxy data by redoubling efforts to curate data according to FAIR (findability, accessibility, interoperability and reusability) data principles. Although palaeoclimate data are more accessible and interoperable than ever, large-scale data analyses, including those

that yield quantitative estimates of global climate indicators and their uncertainties (Table 1), continue to face challenges related to data management and infrastructure[139].

Resolving possible shortcomings in models

If our preferred interpretation is correct and recent global warming was proceeded by a multimillennial global cooling trend, then this points to the need to improve our understanding of natural climate forcings and feedbacks, along with their representation in climate models. The very large seasonal and latitudinal changes in insolation caused by orbital forcing is the most likely instigator of climate feedbacks over the second half of the Holocene. On the proxy side, analysing the response to orbital forcing using records from earlier warm periods and the cyclicities within long palaeorecords will help to further understand both the climate and proxy responses to insolation changes. On the modelling side, further orbital-only model experiments could help to identify responses that are underrepresented in full-forcing simulations at present. Major climate feedbacks that have already received attention include those related to sea ice, monsoon systems and land cover, including anthropogenic influences. More model sensitivity experiments are needed to study the response to dynamic vegetation and dust, with protocols already outlined for PMIP4 (ref. [29]). More work is also needed to analyse large networks of proxy data to identify spatial and temporal patterns of long-term variability that might be attributed to forcing by volcanic aerosols, solar irradiance and the dynamical responses they generate, or those that might reflect yet undiscovered modes of slow variability. This goal also depends on well-curated, readily reusable proxy data.

Furthermore, if our interpretation is correct, the global HTM can provide insight into important climate feedbacks that play out over millennia, as well as potential future impacts of a relatively warm world. Although the HTM is not an analogue for future warming[140], some prominent feedbacks involving the annual cycle are similar for both the HTM and future warming, such as those associated with Arctic amplification[141]. The complex forcings and heterogenous response of Holocene climate serves as a challenging test of climate model performance. As such, a more complete representation of the climate forcings and feedbacks over the Holocene would improve the predictive value of climate models.

Data availability

All of the data used for this Review are from published literature, as cited in the text.

1. Intergovernmental Panel on Climate Change (IPCC). IPCC summary for policymakers. In *Climate Change 2021: The Physical Science Basis. Contribution of Working Group I to the Sixth Assessment Report of the Intergovernmental Panel on Climate Change* (eds Masson-Delmotte, V. et al.) 3–32 (Cambridge Univ. Press, 2021).
2. Fischer, H. et al. Palaeoclimate constraints on the impact of 2 °C anthropogenic warming and beyond. *Nat. Geosci.* **11**, 474–485 (2018).
   Review of warm periods over the past 3.5 million years, including a comparison of proxy data and model simulations and a discussion of climate feedbacks that can enhance warming.
3. Kaufman, D. S. & McKay, N. P. Technical Note: Past and future warming – direct comparison on multi-century timescales. *Clim. Past* **18**, 911–917 (2022).
4. Rockström, J. et al. Planetary boundaries: exploring the safe operating space for humanity. *Ecol. Soc.* **14**, 32 (2019).
5. Lüning, S. & Vahrenholt, F. Paleoclimatological context and reference level of the 2°C and 1.5°C Paris Agreement long-term temperature limits. *Front. Earth Sci.* **5**, 104 (2017).
6. Marcott, S. A., Shakun, J. D., Clark, P. U. & Mix, A. C. A reconstruction of regional and global temperature for the past 11,300 years. *Science* **339**, 1198–1201 (2013).
   The first reconstruction of GMST based on a compilation of globally distributed terrestrial and marine proxy datasets shows evidence for a global HTM. Note: we added 0.3 °C to the GMST reconstructed by Marcott et al. to account for their warmer reference period.
7. Liu, Z. et al. The Holocene temperature conundrum. *Proc. Natl Acad. Sci.* **111**, E3501–E3505 (2014).
   Coined the term 'Holocene temperature conundrum' to describe the mismatch between most climate models that simulate a warming trend during the Holocene, in contrast to proxy data that show gradual cooling during the second half of the Holocene (before industrialization).
8. Bova, S., Rosenthal, Y., Liu, Z., Godad, S. P. & Yan, M. Seasonal origin of the thermal maxima at the Holocene and the last interglacial. *Nature* **589**, 548–553 (2021).
   Presents a large-scale temperature reconstruction, with no global HTM, based on the assumption that sea-surface proxy records are controlled by local seasonal insolation.
9. Thompson, A. J., Zhu, J., Poulsen, C. J., Tierney, J. E. & Skinner, C. B. Northern Hemisphere vegetation change drives a Holocene thermal maximum. *Sci. Adv.* **8**, eabj6535 (2022).
   Experiments using the Community Earth System Model show that expanded Northern Hemisphere vegetation at 6 ka increases GMST by about 0.7 °C, in broad agreement with proxy records.
10. Liu, Y. et al. A possible role of dust in resolving the Holocene temperature conundrum. *Sci. Rep.* **8**, 4434 (2018).
11. Osman, M. B. et al. Globally resolved surface temperatures since the Last Glacial Maximum. *Nature* **599**, 239–244 (2021).
    A data assimilation reconstruction of GMST for the past 24 kyr, based on sea-surface temperatures derived from proxy system models combined with time-slice model simulations, shows slight warming across the middle and late Holocene.
12. Erb, M. P. et al. Reconstructing Holocene temperatures in time and space using paleoclimate data assimilation. *Clim. Past* **18**, 2599–2629 (2022).
    A Holocene data assimilation reconstruction based on the Temp12k database and transient model simulations shows a minor global HTM and cooling between 6 ka and the preindustrial period.
13. Steig, E. J. Mid-Holocene climate change. *Science* **286**, 1485–1487 (1999).
14. Wanner, H., Mercolli, L., Grosjean, M. & Ritz, S. P. Holocene climate variability and change; a data-based review. *J. Geol. Soc.* **172**, 254–263 (2015).
15. Harrison, S. P. et al. Evaluation of CMIP5 palaeo-simulations to improve climate projections. *Nat. Clim. Change* **5**, 735 (2015).
16. Hou, J., Li, C.-G. & Lee, S. The temperature record of the Holocene: progress and controversies. *Sci. Bull.* **64**, 565–566 (2019).
17. Klimenko, V. V., Klimanov, V. A. & Fedorov, M. V. The history of the mean temperature of the Northern Hemisphere over the last 11000 years. *Dokl. Earth Sci.* **348**, 626–629 (1995).
18. Kaufman, D. S. et al. Holocene thermal maximum in the western Arctic (0–180°W). *Quat. Sci. Rev.* **23**, 529–560 (2004).
19. Herzschuh, U. et al. Regional pollen-based Holocene temperature and precipitation patterns depart from the Northern Hemisphere mean trends. Preprint at *EGUsphere* https://doi.org/10.5194/egusphere-2022-127 (2022).
20. Cartapanis, O., Jonkers, L., Moffa-Sanchez, P., Jaccard, S. L. & de Vernal, A. Complex spatio-temporal structure of the Holocene Thermal Maximum. *Nat. Commun.* **13**, 5662 (2022).
21. Crucifix, M., Loutre, M. F., Tulkens, P., Fichefet, T. & Berger, A. Climate evolution during the Holocene: a study with an Earth system model of intermediate complexity. *Clim. Dyn.* **19**, 43–60 (2002).
22. Renssen, H., Seppa, H., Crosta, X., Goosse, H. & Roche, D. M. Global characterization of the Holocene Thermal Maximum. *Quat. Sci. Rev.* **48**, 7–19 (2012).
23. Zhang, Y., Renssen, H., Seppä, H. & Valdes, P. Holocene temperature trends in the extratropical Northern Hemisphere based on inter-model comparisons. *J. Quat. Sci.* **33**, 464–476 (2018).
24. Wright, H. E. Jr et al. (eds) *Global Climates Since the Last Glacial Maximum* (Univ. Minnesota Press, 1993).
25. Lorenz, S. J. et al. Orbitally driven insolation forcing on Holocene climate trends: evidence from alkenone data and climate modeling. *Paleoceanography* **21**, PA1002 (2006).
26. Ljungqvist, F. C. The spatio-temporal pattern of the mid-Holocene thermal maximum. *Geografie* **116**, 91–110 (2011).
27. Wanner, H. Late-Holocene: cooler or warmer? *Holocene* **31**, 1501–1506 (2021).
28. Brierley, C. M. et al. Large-scale features and evaluation of the PMIP4-CMIP6 *midHolocene* simulations. *Clim. Past* **16**, 1847–1872 (2020).
    Mid-Holocene model simulations from the PMIP4 experimental protocol show an ensemble mean GMST change of −0.3 °C relative to preindustrial control runs.
29. Ganopolski, A., Kubatzki, C., Claussen, M., Borvkin, V. & Petoukhov, V. The influence of vegetation-atmosphere-ocean interaction on climate during the mid-Holocene. *Science* **280**, 1916–1919 (1998).
    A coupled atmosphere–ocean–vegetation model shows that, during the mid-Holocene (6 ka), changes in boreal summer insolation, vegetation cover, sea-ice cover and ocean circulation contribute to global HTM.
30. Otto-Bliesner, B. L. et al. The PMIP4 contribution to CMIP6 – part 2: two interglacials, scientific objective and experimental design for Holocene and Last Interglacial simulations. *Geosci. Model Dev.* **10**, 3979–4003 (2017).
31. Chen, D. et al. Framing, context, and methods. In *Climate Change 2021: The Physical Science Basis. Contribution of Working Group I to the Sixth Assessment Report of the Intergovernmental Panel on Climate Change* (eds Masson-Delmotte, V. et al.) 147–286 (Cambridge Univ. Press, 2021).
32. Schmidt, G. A. et al. Using palaeo-climate comparisons to constrain future projections in CMIP5. *Clim. Past* **10**, 221–250 (2014).
33. Kaufman, D. et al. Holocene global mean surface temperature, a multi-method reconstruction approach. *Sci. Data* **7**, 201 (2020).
    Several palaeoclimate reconstruction methods applied to an extensive compilation of terrestrial and marine proxy datasets show a global HTM, followed by global cooling from around 6.5 ka until industrialization (Temp12k reconstruction).
34. Kaufman, D. et al. A global database of Holocene paleotemperature records. *Sci. Data* **7**, 115 (2020).
    A database of quality-controlled, globally distributed temperature proxy datasets used to create the Temp12k reconstruction.
35. Zhang, W., Wu, H., Geng, J. & Cheng, J. Model-data divergence in global seasonal temperature response to astronomical insolation during the Holocene. *Sci. Bull.* **67**, 25–28 (2022).

36. Marcott, S. A., Shakun, J. D., Clark, P. U. & Mix, A. C. A reconstruction of regional and global temperature for the past 11,300 years. *Science* **339**, 1198–1201 (2013).
The first reconstruction of GMST based on a compilation of globally distributed terrestrial and marine proxy datasets shows evidence for a global HTM.
37. Shakun, J. D., Lea, D. W., Lisiecki, L. E. & Raymo, M. E. An 800-kyr record of global surface ocean $\delta^{18}O$ and implications for ice volume-temperature coupling. *Earth Planet. Sci. Lett.* **426**, 58–68 (2015).
38. Huang, S. P., Pollack, H. N. & Shen, P.-Y. A late Quaternary climate reconstruction based on borehole heat flux data, borehole temperature data, and the instrumental record. *Geophys. Res. Lett.* **35**, L13703 (2008).
39. Mann, M. E., Schmidt, G. A., Miller, S. K. & LeGrande, A. N. Potential biases in inferring Holocene temperature trends from long-term borehole information. *Geophys. Res. Lett.* **36**, L05708 (2009).
40. Rao, Z. et al. Pollen data as a temperature indicator in the late Holocene: a review of results on regional, continental and global scales. *Front. Earth Sci.* **10**, 845650 (2022).
41. Zhang, W., Wu, H., Geng, J. & Cheng, J. Model-data divergence in global seasonal temperature response to astronomical insolation during the Holocene. *Sci. Bull.* **67**, 25–28 (2022).
42. Marsicek, J., Shuman, B. N., Bartlein, P. J., Shafer, S. L. & Brewer, S. Reconciling divergent trends and millennial variations in Holocene temperatures. *Nature* **554**, 92–96 (2018).
43. Deevey, E. S. & Flint, R. F. Postglacial hypsithermal interval. *Science* **125**, 182–184 (1957).
44. Gulev, S. K. et al. Changing state of the climate system. In *Climate Change 2021: The Physical Science Basis. Contribution of Working Group I to the Sixth Assessment Report of the Intergovernmental Panel on Climate Change* (eds Masson-Delmotte, V. et al.) 287–422 (Cambridge Univ. Press, 2021).
45. Oerlemans, J. & Reichert, B. K. Relating glacier mass balance to meteorological data by using a seasonal sensitivity characteristic. *J. Glaciol.* **46**, 1–6 (2000).
46. Leclercq, P. W. & Oerlemans, J. Global and hemispheric temperature reconstruction from glacier length fluctuations. *Clim. Dyn.* **38**, 1065–1079 (2012).
47. Solomina, O. N. et al. Holocene glacier fluctuations. *Quat. Sci. Rev.* **111**, 9–34 (2015).
48. Porter, S. C. Neoglaciation in the American Cordilleras. in *Encyclopedia of Quaternary Science* (ed. Elias, S. A.) 1133–1142 (Elsevier, 2007).
49. Porter, S. C. & Denton, G. H. Chronology of neoglaciation in the North American Cordillera. *Am. J. Sci.* **265**, 177–210 (1967).
50. Briner, J. P. et al. Holocene climate change in Arctic Canada and Greenland. *Quat. Sci. Rev.* **147**, 340–364 (2016).
51. Kingslake, J. et al. Extensive retreat and re-advance of the West Antarctic Ice Sheet during the Holocene. *Nature* **558**, 430–434 (2018).
52. Baggenstos, D. et al. Earth's radiative imbalance from the Last Glacial Maximum to the present. *Proc. Natl Acad. Sci.* **116**, 14881–14886 (2019).
53. Rosenthal, Y., Kalansky, J., Morley, A. & Linsley, B. A paleo-perspective on ocean heat content: lessons from the Holocene and Common Era. *Quat. Sci. Rev.* **155**, 1–12 (2017).
54. Bereiter, B., Shackleton, S., Baggenstos, D., Kawamura, K. & Seeringhaus, J. Mean global ocean temperatures during the last glacial transition. *Nature* **553**, 39–44 (2018).
55. Matthews, J. A. & Briffa, K. R. The 'Little Ice Age': re-evaluation of an evolving concept. *Geogr. Ann. A Phys. Geogr.* **87**, 17–36 (2005).
56. McGregor, H. V. et al. Robust global ocean cooling trend for the pre-industrial Common Era. *Nat. Geosci.* **8**, 671–677 (2015).
57. PAGES 2k Consortium. Continental-scale temperature variability during the past two millennia. *Nat. Geosci.* **6**, 339–346 (2013).
58. PAGES 2k Consortium. A global multiproxy database for temperature reconstructions of the Common Era. *Sci. Data* **4**, 170088 (2017).
59. Solomina, O. N. et al. Glacier fluctuations during the past 2000 years. *Quat. Sci. Rev.* **149**, 61–90 (2016).
60. Cuesta-Valero, F. J., Garcia-Garcia, A., Beltrami, H., González-Rouco, J. F. & Garcia-Bustamante, E. Long-term global ground heat flux and continental heat storage from geothermal data. *Clim. Past* **17**, 451–468 (2021).
61. Laskar, J. et al. A long-term numerical solution for the insolation quantities of the Earth. *Astron. Astrophys.* **428**, 261–285 (2004).
62. Lorenz, S. J. & Lohman, G. Acceleration technique for Milankovitch type forcing in a coupled atmosphere-ocean circulation model: method and application for the Holocene. *Clim. Dyn.* **23**, 727–743 (2004).
63. Lindén, M., Möller, P. E. R., Björck, S. & Sandgren, P. E. R. Holocene shore displacement and deglaciation chronology in Norrbotten, Sweden. *Boreas* **35**, 1–22 (2006).
64. Ullman, D. J. et al. Final Laurentide ice-sheet deglaciation and Holocene climate-sea level change. *Quat. Sci. Rev.* **152**, 49–59 (2016).
65. Routson, C. et al. Mid-latitude net precipitation decrease with Arctic warming during the Holocene. *Nature* **568**, 83–87 (2019).
66. Meyer, H. et al. Long-term winter warming trend in the Siberian Arctic during the mid- to late Holocene. *Nat. Geosci.* **8**, 122–125 (2015).
67. Baker, J., Lachniet, M., Chervyatsova, O., Asmerom, Y. & Polyak, V. J. Holocene warming in western continental Eurasia driven by glacial retreat and greenhouse forcing. *Nat. Geosci.* **10**, 430–435 (2017).
68. Holland, K. M., Porter, T. J., Froese, D. G., Kokelj, S. V. & Buchanan, C. A. Ice-wedge evidence of Holocene winter warming in the Canadian Arctic. *Geophys. Res. Lett.* **47**, e2020GL087942 (2020).
69. Longo, W. M. et al. Insolation and greenhouse gases drove Holocene winter and spring warming in Arctic Alaska. *Quat. Sci. Rev.* **242**, 106438 (2020).
70. Zhang, W. et al. Holocene seasonal temperature evolution and spatial variability over the Northern Hemisphere landmass. *Nat. Commun.* **13**, 5334 (2022).
71. Mantsis, D. F., Clement, A. C., Broccoli, A. J. & Erb, M. P. Climate feedbacks in response to changes in obliquity. *J. Clim.* **24**, 2830–2845 (2011).
72. Laepple, T. & Lohmann, G. Seasonal cycle as template for climate variability on astronomical timescales. *Paleoceanography* **24**, PA4201 (2009).
73. Prentice, I. C. & Jolly, D. BIOME 6000 participants. Mid-Holocene and glacial-maximum vegetation geography of the northern continents and Africa. *J. Biogeogr.* **27**, 507–519 (2000).
74. Cao, X., Tian, F., Dallmeyer, A. & Herzschuh, U. Northern Hemisphere biome changes (>30°N) since 40 cal ka BP and their driving factors inferred from model-data comparisons. *Quat. Sci. Rev.* **220**, 291–309 (2019).
75. Dallmeyer, A. et al. Holocene vegetation transitions and their climatic drivers in MPI-ESM1.2. *Clim. Past* **17**, 2481–2513 (2021).
76. O'ishi, R. & Abe-Ouchi, A. Polar amplification in the mid-Holocene derived from dynamical vegetation change with a GCM. *Geophys. Res. Lett.* **38**, L14702 (2011).
77. Diffenbaugh, N. S. & Sloan, L. C. Global climate sensitivity to land surface change: the Mid Holocene revisited. *Geophys. Res. Lett.* **29**, 1476 (2002).
78. He, F. et al. Simulating global and local surface temperature changes due to Holocene anthropogenic land cover change. *Geophys. Res. Lett.* **41**, 623–631 (2014).
79. Albani, S. et al. Twelve thousand years of dust: the Holocene global dust cycle constrained by natural archives. *Clim. Past* **11**, 869–903 (2015).
80. Liu, Y. et al. A possible role of dust in resolving the Holocene temperature conundrum. *Sci. Rep.* **8**, 4434 (2018).
81. Zhang, M., Liu, Y., Zhang, J. & Wen, Q. AMOC and climate responses to dust reduction and greening of the Sahara during the mid-Holocene. *J. Clim.* **34**, 4893–4912 (2021).
82. Hopcroft, P. O. & Valdes, P. J. On the role of dust-climate feedbacks during the mid-Holocene. *Geophys. Res. Lett.* **46**, 1612–1621 (2019).
83. Braconnot, P. et al. Impact of dust in PMIP-CMIP6 mid-Holocene simulations with the IPSL model. *Clim. Past* **17**, 1091–1117 (2021).
84. Serreze, M. C. & Barry, R. G. Processes and impacts of Arctic amplification: a research synthesis. *Glob. Planet. Change* **77**, 85–96 (2011).
85. Stranne, C., Jakobsson, M. & Björk, G. Arctic Ocean perennial sea ice breakdown during the early Holocene insolation maximum. *Quat. Sci. Rev.* **92**, 123–132 (2014).
86. Funder, S. et al. A 10,000-year record of Arctic Ocean sea-ice variability—view from the beach. *Science* **333**, 747–750 (2011).
87. de Vernal, A. et al. Natural variability of Arctic Ocean sea ice during the present interglacial. *Proc. Natl Acad. Sci.* **117**, 26069–26075 (2020).
88. Wolff, E. W. et al. Southern Ocean sea-ice extent, productivity and iron flux over the past eight glacial cycles. *Nature* **440**, 491–496 (2006).
89. Crosta, X. et al. Antarctic sea ice over the past 130 000 years – part 1: a review of what proxy records tell us. *Clim. Past* **18**, 1729–1756 (2022).
90. Park, H.-S., Kim, S.-J., Stewart, A. L., Son, S.-W. & Seo, K.-H. Mid-Holocene Northern Hemisphere warming driven by Arctic amplification. *Sci. Adv.* **5**, eaax8203 (2019).
Model simulations show that, during the mid-Holocene (6 ka), mean annual temperature in the Northern Hemisphere increased in response to reduced Arctic sea-ice extent.
91. Chen, J., Zhang, Q., Kjellström, E., Lu, Z. & Chen, F. The contribution of vegetation-climate feedback and resultant sea ice loss to amplified Arctic warming during the mid-Holocene. *Geophys. Res. Lett.* **49**, e2022GL098816 (2022).
92. Bader, J. et al. Global temperature modes shed light on the Holocene temperature conundrum. *Nat. Commun.* **11**, 4726 (2020).
93. Tomas, R. A., Deser, C. & Sun, L. The role of ocean heat transport in the global climate response to projected Arctic sea ice loss. *J. Clim.* **29**, 6841–6859 (2016).
94. Blackport, R. & Kushner, P. J. The role of extratropical ocean warming in the coupled climate response to Arctic sea ice loss. *J. Clim.* **31**, 9193–9206 (2018).
95. Hudson, S. R. Estimating the global radiative impact of the sea ice–albedo feedback in the Arctic. *J. Geophys. Res. Atmos.* **116**, D16102 (2011).
96. England, M. R., Polvani, L. M., Sun, L. & Deser, C. Tropical climate responses to projected Arctic and Antarctic sea-ice loss. *Nat. Geosci.* **13**, 275–281 (2020).
97. Wunderling, N., Willeit, M., Donges, J. F. & Winkelmann, R. Global warming due to loss of large ice masses and Arctic summer sea ice. *Nat. Commun.* **11**, 5177 (2020).
98. Tierney, J. E. et al. Past climates inform our future. *Science* **370**, eaay3701 (2020).
99. Köhler, P., Nehrbass-Ahles, C., Schmitt, J., Stocker, T. F. & Fischer, H. A 156 kyr smoothed history of the atmospheric greenhouse gases CO_2, CH_4, and N_2O and their radiative forcing. *Earth Syst. Sci. Data* **9**, 363–387 (2017).
100. Brovkin, V. et al. What was the source of the atmospheric CO_2 increase during the Holocene? *Biogeosciences* **16**, 2543–2555 (2019).
101. Ruddiman, W. F. et al. Late Holocene climate: natural or anthropogenic? *Rev. Geophys.* **54**, 93–118 (2016).
102. Tzedakis, P. C., Channell, J. E. T., Hodell, D. A., Kleiven, H. F. & Skinner, L. C. Determining the natural length of the current interglacial. *Nat. Geosci.* **5**, 138–141 (2012).
103. Abram, N. J. et al. Early onset of industrial-era warming across the oceans and continents. *Nature* **536**, 411–418 (2016).
104. Shindell, D. T., Schmidt, G. A., Miller, R. L. & Mann, M. E. Volcanic and solar forcing of climate change during the preindustrial era. *J. Clim.* **16**, 4094–4107 (2003).
105. PAGES 2k Consortium. Consistent multidecadal variability in global temperature reconstructions and simulations over the Common Era. *Nat. Geosci.* **12**, 643–649 (2019).
106. Wu, C.-J., Krivova, N. A., Solanki, S. K. & Usoskin, I. G. Solar total and spectral irradiance reconstruction over the last 9000 years. *Astron. Astrophys.* **620**, A120 (2018).
107. Forster, P. et al. The Earth's energy budget, climate feedbacks, and climate sensitivity. In *Climate Change 2021: The Physical Science Basis. Contribution of Working Group I to the Sixth Assessment Report of the Intergovernmental Panel on Climate Change* (eds Masson-Delmotte, V. et al.) 923–1054 (Cambridge Univ. Press, 2021).
108. Gray, L. J. et al. Solar influences on climate. *Rev. Geophys.* **48**, RG4001 (2010).
109. Soon, W. A review of Holocene solar-linked climatic variation on centennial to millennial timescales: physical processes, interpretative frameworks and a new multiple cross-wavelet transform algorithm. *Earth Sci. Rev.* **134**, 1–15 (2014).
110. Lu, W. et al. Temporal and spatial response of Holocene temperature to solar activity. *Quat. Int.* **613**, 39–45 (2022).
111. Wanner, H. et al. Mid- to late Holocene climate change: an overview. *Quat. Sci. Rev.* **27**, 1791–1828 (2008).
A review of middle to late Holocene climate change, summarizing key climate forcings and evidence from both proxies and models.
112. Mayewski, P. A. et al. Holocene climate variability. *Quat. Res.* **62**, 243–255 (2004).

113. Traversi, R. et al. Nitrate in polar ice: a new tracer of solar variability. *Sol. Phys.* **280**, 237–254 (2012).
114. Sigl, M., Toohey, M., McConnell, J. R., Cole-Dai, J. & Severi, M. Volcanic stratospheric sulfur injections and aerosol optical depth during the Holocene (past 11,500 years) from a bipolar ice core array. *Earth Syst. Sci. Data* **14**, 3167–3196 (2022).
115. Schneider, D. P., Ammann, C. M., Otto-Bliesner, B. L. & Kaufman, D. S. Climate response to large, high-latitude and low-latitude volcanic eruptions in the Community Climate System Model. *J. Geophys. Res. Atmos.* **114**, D15101 (2009).
116. Miller, G. H. et al. Abrupt onset of the Little Ice Age triggered by volcanism and sustained by sea-ice/ocean feedbacks. *Geophys. Res. Lett.* **39**, L02708 (2012).
117. Gupta, M. & Marshall, J. The climate response to multiple volcanic eruptions mediated by ocean heat uptake: damping processes and accumulation potential. *J. Clim.* **31**, 8669–8687 (2018).
118. Lohmann, G., Pfeiffer, M., Laepple, T., Leduc, G. & Kim, J.-H. A model–data comparison of the Holocene global sea surface temperature evolution. *Clim. Past* **9**, 1807–1839 (2013).
119. Zhang, Q. et al. Climate change between the mid and late Holocene in northern high latitudes – part 2: model-data comparisons. *Clim. Past* **6**, 609–626 (2010).
120. Shakun, J. D. & Carlson, A. E. A global perspective on Last Glacial Maximum to Holocene climate change. *Quat. Sci. Rev.* **29**, 1801–1816 (2010).
121. Zhang, X. & Chen, F. Non-trivial role of internal climate feedback on interglacial temperature evolution. *Nature* **600**, E1–E3 (2021).
122. Laepple, T., Shakun, J., He, F. & Marcott, S. Concerns of assuming linearity in the reconstruction of thermal maxima. *Nature* **607**, E12–E14 (2022).
123. Bova, S. et al. Reply to: Non-trivial role of internal climate feedback on interglacial temperature evolution. *Nature* **600**, E4–E6 (2021).
124. Bova, S. et al. Reply to: Concerns of assuming linearity in the reconstruction of thermal maxima. *Nature* **607**, E15–E18 (2022).
125. Annan, J. D., Hargreaves, J. C. & Mauritsen, T. A new global surface temperature reconstruction for the Last Glacial Maximum. *Clim. Past* **18**, 1883–1896 (2022).
126. King, J. et al. A data assimilation approach to last millennium temperature field reconstruction using a limited high-sensitivity proxy network. *J. Clim.* **34**, 7091–7111 (2021).
127. Johnson, J. S. et al. Review article: Existing and potential evidence for Holocene grounding line retreat and readvance in Antarctica. *Cryosphere* **16**, 1543–1562 (2022).
128. Jones, R. S. et al. Stability of the Antarctic ice sheet during the pre-industrial Holocene. *Nat. Rev. Earth Environ.* **3**, 500–515 (2022).
129. Kopp, R. E. et al. Temperature-driven global sea-level variability in the Common Era. *Proc. Natl Acad. Sci.* **113**, E1434–E1441 (2016).
130. Lambeck, K., Rouby, H., Purcell, A., Sun, Y. & Sambridge, M. Sea level and global ice volumes from the Last Glacial Maximum to the Holocene. *Proc. Natl Acad. Sci.* **111**, 15296–15303 (2014).
131. Milne, G. A. & Mitrovica, J. X. Searching for eustasy in deglacial sea-level histories. *Quat. Sci. Rev.* **27**, 2292–2302 (2008).
132. Vacchi, M. et al. Multiproxy assessment of Holocene relative sea-level changes in the western Mediterranean: sea-level variability and improvements in the definition of the isostatic signal. *Earth Sci. Rev.* **155**, 172–197 (2016).
133. Meco, J. et al. Mid and late Holocene sea level variations in the Canary Islands. *Palaeogeogr. Palaeoclimatol. Palaeoecol.* **507**, 214–225 (2018).
134. Crawford, O. Quantifying the sensitivity of post-glacial sea level change to laterally varying viscosity. *Geophys. J. Int.* **214**, 1324–1363 (2018).
135. Kwiecien, O. et al. What we talk about when we talk about seasonality – a transdisciplinary review. *Earth Sci. Rev.* **225**, 103843 (2022).
136. Evans, M. N., Talwinski-Ward, S. E., Thompson, D. M. & Anchukaitis, K. J. Applications of proxy system modeling in high resolution paleoclimatology. *Quat. Sci. Rev.* **76**, 16–28 (2013).
137. Dee, S. G., Steiger, N. J., Emile-Geay, J. & Hakim, G. J. On the utility of proxy system models for estimating climate states over the common era. *J. Adv. Model. Earth Syst.* **8**, 1164–1179 (2016).
138. Wörmer, L. et al. Ultra-high-resolution paleoenvironmental records via direct laser-based analysis of lipid biomarkers in sediment core samples. *Proc. Natl Acad. Sci.* **111**, 15669–15674 (2014).
139. Williams, J. W., Kaufman, D. S., Newton, A. & von Gunten, L. Building open data: data stewards and community-curated data resources. *PAGES Mag.* **26**, 50–51 (2018).
140. Mitchell, J. F. B. Greenhouse warming: is the mid-Holocene a good analogue? *J. Clim.* **3**, 1177–1192 (1990).
141. Yoshimori, M. & Suzuki, M. The relevance of mid-Holocene Arctic warming to the future. *Clim. Past* **15**, 1375–1394 (2019).
142. Peltier, W. R. Global glacial isostasy and the surface of the ice-age Earth: the ICE-5G (VM2) model and GRACE. *Annu. Rev. Earth Planet. Sci.* **32**, 111–1149 (2004).
143. Rosenthal, Y., Linsley, B. K. & Oppo, D. W. Pacific Ocean heat content during the past 10,000 years. *Science* **342**, 617–621 (2013).

Acknowledgements We thank our colleagues for their helpful input, including D. Baggenstos, S. Bova, R. Bradley, C. Brierley, R. Creel, S. Dee, M. Erb, H. Fischer, O. Heiri, U. Herzschuh, P. Hopcroft, T. Laepple, D. Lunt, N. McKay, M. Osman and A. Thompson. This Review was motivated by the need for a comprehensive assessment of palaeo GMST for the IPCC's Sixth Assessment Report.

Author contributions D.S.K. conceived the Review, assembled the datasets and wrote the first manuscript. E.B. expanded and improved the manuscript and crafted the figures.

Competing interests The authors declare no competing interests.

Additional information
Correspondence and requests for materials should be addressed to Darrell S. Kaufman.
Peer review information *Nature* thanks Samantha Bova, Oliver Heiri, Peter Hopcroft and the other, anonymous, reviewer(s) for their contribution to the peer review of this work.
Reprints and permissions information is available at http://www.nature.com/reprints.
Publisher's note Springer Nature remains neutral with regard to jurisdictional claims in published maps and institutional affiliations.